TÜBİTAK

Turkish Journal of Chemistry

http://journals.tubitak.gov.tr/chem/

Research Article

Turk J Chem
(2016) 40: 784 – 801

doi:10.3906/kim-1602-59

Degradation of bisphenol-a using a sonophoto Fenton-like hybrid process over a $LaFeO_3$ perovskite catalyst and a comparison of its activity with that of a TiO_2 photocatalyst

Meral DÜKKANCI*
Department of Chemical Engineering, Faculty of Engineering, Ege University, Bornova, İzmir, Turkey

Received: 17.02.2016 • **Accepted/Published Online:** 04.05.2016 • **Final Version:** 02.11.2016

Abstract: Oxidation of bisphenol-A (BPA) was investigated using a sonophoto Fenton-like hybrid process under visible light irradiation in the presence of iron-containing perovskite $LaFeO_3$ catalysts. For this purpose, firstly the perovskite catalyst ($LaFeO_3$) was prepared by the sol-gel method and calcined at different temperatures (500, 700, and 800 °C). The prepared catalysts were characterized using XRD, SEM, FTIR, nitrogen adsorption, UV-vis DRS, and ICP/OES measurements.

Among the prepared catalysts the catalyst that was calcined at 500 °C showed better catalytic activity with respect to degradation and chemical oxygen demand (COD) reduction (of 21.8% and 11.2%, respectively, after 3 h of reaction duration) than the other catalysts calcined at 700 °C and 800 °C. The catalytic activity of the $LaFeO_3$ perovskite catalyst calcined at 500 °C was compared with that of a TiO_2 photocatalyst containing Fe and prepared by the sol-gel method. Better photocatalytic activity in terms of degradation of BPA, total organic carbon (TOC), and COD reductions was observed with the $LaFeO_3$ perovskite catalyst under visible light.

The degradation, COD, and TOC reductions after 6 h of oxidation were 34.8%, 26.9%, and 8.8% for the $LaFeO_3$ perovskite catalyst, and 33.1%, 19.7%, and 4.9% for the Fe/TiO_2 catalyst, respectively.

Key words: Bisphenol-A, sonophoto Fenton-like process, hybrid advanced oxidation process, perovskite catalyst

1. Introduction

Bisphenol-A (BPA) is a well-known endocrine disturbing compound that is widely used in the manufacture of epoxy and polycarbonate plastics, dental sealants, coating of cans, flame retardants, thermal papers, printing ink, and antioxidants.[1,2] The source of human exposure to BPA is food and liquid storage containers. BPA is released into the environment through either sewage treatment effluent (via human-ingested BPA being eliminated through sewage), landfill leachate (via hydrolysis of BPA from plastics), natural degradation of polycarbonate plastics, or wastewaters from the production steps of related products that contain BPA. BPA can leach from polycarbonate plastic when exposed to heat.[3] However, BPA plays a role in thyroid hormone dysfunctions, central nervous system function disorder, and immune suppression.[4,5] BPA is also acutely toxic in the range of about 1–10 $\mu g/cm^3$ for a number of freshwater and marine species. Due to the reasons given above, BPA-containing wastewater must be treated before discharge into the environment. However, some of the treatment methods require a long treatment time (biochemical treatment), and generate considerable amounts

*Correspondence: meral.dukkanci@ege.edu.tr

of sludge (electrochemical technique) and secondary pollutants (adsorption). Biochemical treatment is not capable of removing BPA completely.[3] Because of all these reasons, it is necessary to use an effective treatment process for the removal of BPA from wastewater. Several alternative processes have been proposed. Of all the methods developed so far, the advanced oxidation processes (AOPs) offer several particular advantages in terms of unselective degradation of BPA into a final mineralized form with the production of a highly oxidative hydroxyl radical ($OH^{\cdot}$).[6]

In the present study, sonophoto Fenton-like hybrid oxidation (sonication-assisted heterogeneous photo-Fenton–like process) technology was used for the degradation of a BPA aqueous solution. In the Fenton oxidation, a powerful source of oxidative $HO^{\cdot}$ radicals is generated from the H_2O_2 in the presence of Fe^{2+} ions. The generated $HO^{\cdot}$ radicals are highly oxidative, nonselective, and are able to decompose many organic compounds including phenolic compounds. However, homogeneous Fenton oxidation has some drawbacks; for example, the amount of iron used in the homogeneous Fenton process is above the European Union limits. Thus, the wastewater cannot be discharged with the Fe used. In addition, treatment of the sludge containing iron is not economical and it requires manpower and chemicals, and also a strict control of pH around 2–3 is required. These drawbacks can be overcome by using heterogeneous Fenton-type catalysts.[7]

In the Fenton-like oxidation, Fe^{3+} in the catalyst is reduced into Fe^{2+} with generation of $HO_2^{\cdot}$ radicals, which are less reactive than $OH^{\cdot}$ radicals (Eq. (1)). This reaction is followed by an Fe^{3+} regeneration step with following of the $HO^{\cdot}$ radicals (Eq. (2)). Similar to all AOPs, the produced $OH^{\cdot}$ radicals react with organic pollutants (here BPA):

$$X - Fe^{3+} + H_2O_2 \rightarrow X - Fe^{2+} + HO_2^{\cdot} + H^+ \tag{1}$$

$$X - Fe^{2+} + H_2O_2 \rightarrow X - Fe^{3+} + OH^- + HO^{\cdot}, \tag{2}$$

where X represents the surface of the catalyst.[8]

Photoreactions do not occur on illumination with light alone. These reactions often require the use of a photocatalyst. Among the various photocatalysts, TiO_2 has been extensively studied as a semiconductor photocatalyst because of its relatively high photocatalytic activity, chemical stability, low cost, and environmental friendliness. However, TiO_2 is only active under UV light irradiation due to its large band gap energy (3.2 eV), which results in low efficiency in the use of solar light.[9–11] The photostability of the metal halides such as AgCl and AgBr is poor due to the cleavage of the metal–halide bond under irradiation. The metal sulfides also suffer from photocorrosion.[12]

However, iron-containing perovskite catalysts can be used as either photocatalysts (under visible light) or heterogeneous Fenton-like catalysts; the synergetic effect between the photocatalytic and Fenton reaction may further accelerate the degradation of pollutants.[13,14] Perovskite catalysts have attracted considerable attention due to their high catalytic activity, low cost, and environmental friendliness. For these reasons, in this study, an iron-containing $LaFeO_3$ perovskite catalyst was used.

In the photocatalytic degradation in the presence of $LaFeO_3$, with visible light ($\lambda > 400$ nm) illumination, photogenerated electron-hole pairs are formed in the $LaFeO_3$ perovskite catalyst (Eq. (3)). Thus the electrons are easily trapped by the H_2O_2, forming $OH^{\cdot}$ radicals (Eq. (4)), which degrade the organic pollutant into intermediates products and then CO_2 and water according to reaction conditions studied (Eq. (5)):[14]

$$LaFeO_3 + h\upsilon \rightarrow e_{cb}^- + h_{vb}^+ \tag{3}$$

$$H_2O_2 + LaFeO_3(e_{cb}^-) \rightarrow OH^{\cdot} + OH^- \quad (4)$$

$$BPA + OH^{\cdot} \rightarrow \text{ intermediates } \rightarrow CO_2 \text{ and water}, \quad (5)$$

where hv represents the visible light illumination.

The other AOP used in this project was sonication. Sonication of aqueous solutions provokes the formation and collapse of cavitation bubbles. During the collapse of cavitation bubbles, theoretically it has been shown that the temperature inside the cavity could reach about 5000 K and 1900 K in the interfacial region between the solution and the collapsing bubbles. Moreover, the effective pressure is around 1000 atm at the hot spot and the life time of hot spot is under 1 μs.[15] These high-energy phenomena cause degradation of organic compounds in aqueous solutions. The heat from the cavity collapse decomposes water into extremely reactive hydrogen atoms ($H^{\cdot}$) and hydroxyl radicals ($OH^{\cdot}$). Hydroxyl radicals recombine to form hydrogen peroxide (H_2O_2) and hydrogen atoms recombine to form molecular hydrogen (H_2) (Eqs. (6)–(9)).

$$H_2O))) \rightarrow OH^{\cdot} + H^{\cdot} (\text{Thermolysis}) \quad (6)$$

$$OH^{\cdot} + H^{\cdot} \rightarrow H_2O \quad (7)$$

$$OH^{\cdot} + OH^{\cdot} \rightarrow H_2O_2 \quad (8)$$

$$2H^{\cdot} \rightarrow H_2, \quad (9)$$

where))) refers to the application of ultrasound.[15]

In the sonication, the degradation proceeds mainly by two reaction mechanisms: direct pyrolysis in and around the collapsing bubbles (thermal decomposition due to high temperature in and around the cavitation bubble) and oxidation by $OH^{\cdot}$ radicals (formed from Eq. (6)).[15]

Performing the photocatalytic reaction with sonication increases the oxidation rate with the increased generation of $OH^{\cdot}$ radicals (Eq. (6)) and reduces the mass transfer limitations with the turbulence created by sonication. Sonication also helps in the cleaning of the catalyst surface, which increases its efficiency. In addition, the formed H_2O_2 via reaction (8) in sonication can react with Fe^{2+} in the catalyst to form $OH^{\cdot}$ radicals (sono-Fenton process).

In the literature, there are several studies on the degradation of BPA by AOPs used individually or in combination with each other, such as sonication,[16,17] comparative oxidation of sonication and homogeneous Fenton reaction,[18] sono-Fenton reaction,[19,20] photo-Fenton reaction,[21] sorption on the goethite,[22] photooxidation,[23,24] photocatalytic degradation in the presence of TiO_2 catalysts,[25–28] ozone+UV oxidation,[29] ozonation,[30,31] sonophotocatalytic oxidation,[32,33] homogeneous Fenton oxidation,[34] oxidation over a $SrFeO_{3-\delta}$ perovskite catalyst in the dark,[35] and H_2O_2-assisted photoelectrocatalytic oxidation.[36] In the photocatalytic degradation of BPA under visible light, C–N codoped TiO_2, Bi_2WO_6, magnetic $BiOBr@SiO_2@Fe_3O_4$, a graphene-oxide/$AgPO_4$ composite, and a mesopolymer modified with palladium phthalocyaninesulfonate catalysts were reported in the literature.[37–41]

However, to the best of our knowledge, there is no study on the heterogeneous sonophoto Fenton-like oxidation of BPA. In addition, this study is the first on the heterogeneous sonophoto Fenton-like oxidation

of BPA over a $LaFeO_3$ perovskite catalyst under visible light. The comparison of activities of the $LaFeO_3$ perovskite and Fe/TiO_2 catalysts under visible light irradiation is also a good contribution to the related literature.

2. Results and discussion

2.1. Catalyst characterization

The powder X-ray diffraction (XRD) patterns of the catalysts were recorded in the range of 10–80 ° with a Philips X'Pert Pro with Cu-Kα radiation to determine the crystalline structure of the samples. The morphological properties were analyzed with a scanning electron microscope (FEI Quanta250 FEG). The nitrogen adsorption isotherms at 77 K were measured using the Micromeritics ASAP 2010. Before the adsorption measurements, samples were degassed at 573 K under vacuum. The FT-IR spectra were recorded at 400–4000 cm^{-1} with a PerkinElmer Spectrum 100 spectrometer with 1/100 KBr pellets. The content of iron in the samples was determined with a Thermo Scientific/ICAP5000 ICP-OES spectrophotometer. The band gap energy value measurements were recorded using a UV-Vis DRS/Shimadzu 2600 with ISR apparatus.

The prepared samples were denoted as $LaFeO_3$-500, $LaFeO_3$-700, and $LaFeO_3$-800, respectively, for the calcination temperatures of 500, 700, and 800 °C.

2.1.1. X-ray diffraction studies

The XRD patterns of the $LaFeO_3$ perovskite samples calcined at the three calcination temperatures are displayed in Figure 1.

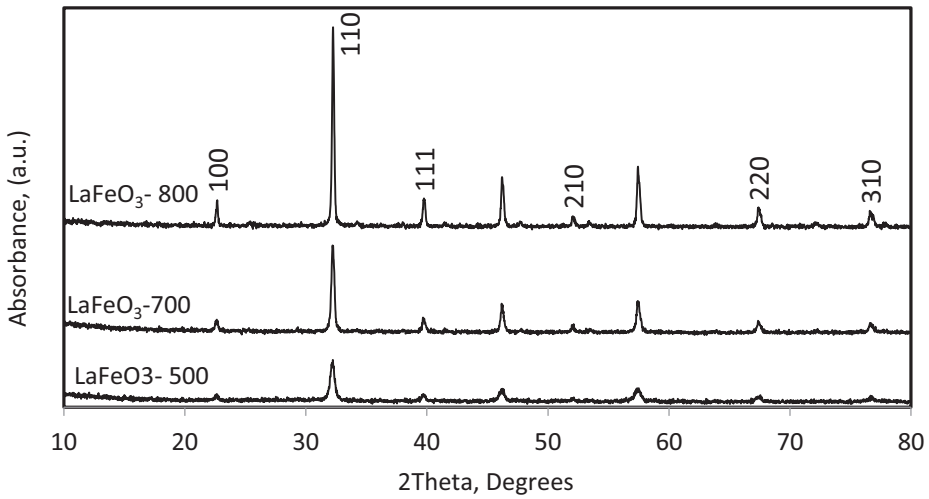

Figure 1. XRD patterns of the prepared catalysts at different calcination temperatures.

According to the XRD analysis, the intensive peaks of three samples at 2θ of 22.63°, 32.22°, 39.73°, 46.21°, 57.45°, 67.42°, 72.12°, and 76.69° represent the main features of the perovskite materials, which are in accordance with the literature.[13,42–44] The samples calcined at 500, 700, and 800 °C yield a well-crystallized pure $LaFeO_3$ phase (JCPDS file no. 75-0541) with a cubic structure.[45,46] As the calcination temperature increased, the peak intensity increased and the peaks became narrower. This result showed the increment of the crystalline structure of the $LaFeO_3$ perovskite.

As seen from Figure 1, there is no impurity in the $LaFeO_3$ perovskite catalyst calcined at the three different temperatures.

Figure 2 shows the XRD peaks of the $LaFeO_3$ perovskite catalyst calcined at 500 °C, and in addition Fe_2O_3 (Figure 2a) and La_2O_3 (Figure 2b) are shown for comparison.

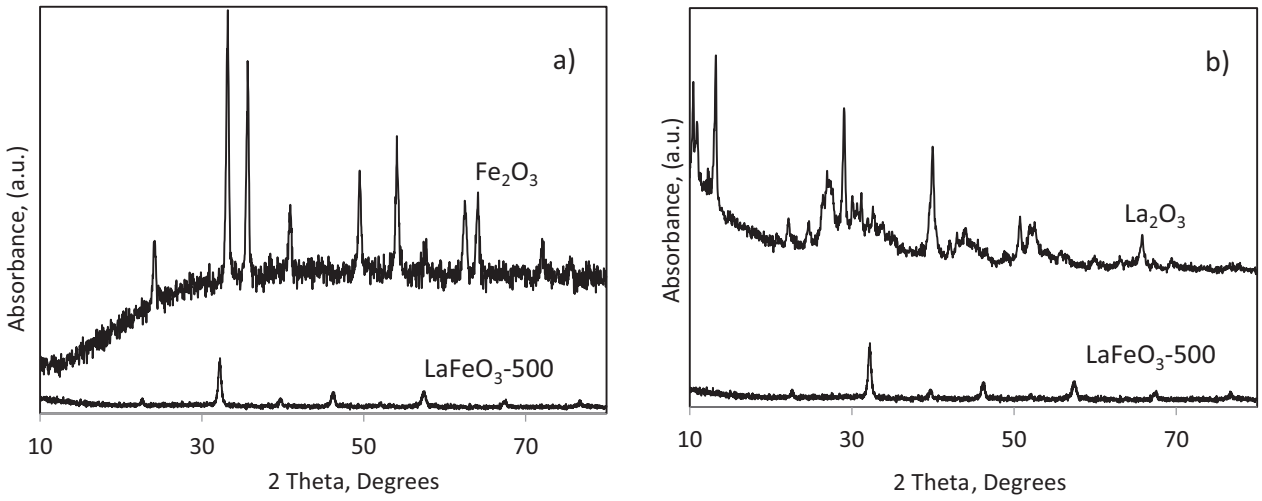

Figure 2. XRD patterns of a) Fe_2O_3 and b) La_2O_3 samples.

When the XRD peaks of the $LaFeO_3$ perovskite and Fe_2O_3 are compared, it may be concluded that the $LaFeO_3$ did not contain Fe_2O_3 in the structure (Figure 2a). Similarly, it was seen that there was no La_2O_3 in the $LaFeO_3$ perovskite structure (Figure 2b). Whether the perovskite catalyst contained Fe_2O_3/La_2O_3 or not was examined by FTIR analysis and is given in Part 2.1.2.

The tolerance factor of the ABO_3 perovskite catalysts shows the stability of the catalyst theoretically. The tolerance factor (t) of the ABO_3 is calculated using Eq. (10):

$$t = \frac{(r_A + r_O)}{\sqrt{2}\,(r_B + r_O)}, \tag{10}$$

where r_A, r_B, and r_O, are the radii for the La, Fe, and O ions, respectively. The tolerance factor of ideal perovskite is 1; when the tolerance factor of the ABO_3 perovskite structure is between 0.75 and 1.0, the ABO_3 compounds have a stable perovskite structure. The tolerance factor of the $LaFeO_3$ perovskite catalysts is given as 0.86.[42] This means that the prepared catalysts are stable theoretically and have single phase perovskite structures.

The crystallite sizes (C_s) of the catalysts were calculated from the half-height width of the peaks at 2θ of 32.22° using the Scherrer equation:[47]

$$C_s = \frac{K\lambda}{\beta\cos\theta}, \tag{11}$$

where β = line width at half maximum height, θ = diffraction angle, K = shape factor of 0.9, and λ = the wave length of the X-ray radiation (CuKα = 0.15405 nm).

Based on the Scherrer equation, the calculated crystallite sizes (C_s) of the catalysts are given in Table 1.

Table 1. Crystal sizes of the prepared catalysts.

Catalyst	Crystallite sizes (C_s), nm
$LaFeO_3$-500	19.69
$LaFeO_3$-700	28.51
$LaFeO_3$-800	41.35

As seen in Table 1, increasing the calcination temperature caused growth of the nanocrystallites and the crystal size increased from 19.69 nm to 28.51 nm and to 41.35 nm as the calcination temperature increased from 500 to 700 and to 800 °C, respectively.

2.1.2. FT-IR measurements

FT-IR spectra of the catalyst samples ($LaFeO_3$ (calcined at three different temperatures), Fe_2O_3 and La_2O_3) are depicted in Figure 3 in the range of 400–4000 cm^{-1}. Figure 3 also shows the FT-IR spectra of catalyst used after the sonophoto Fenton-like oxidation of BPA.

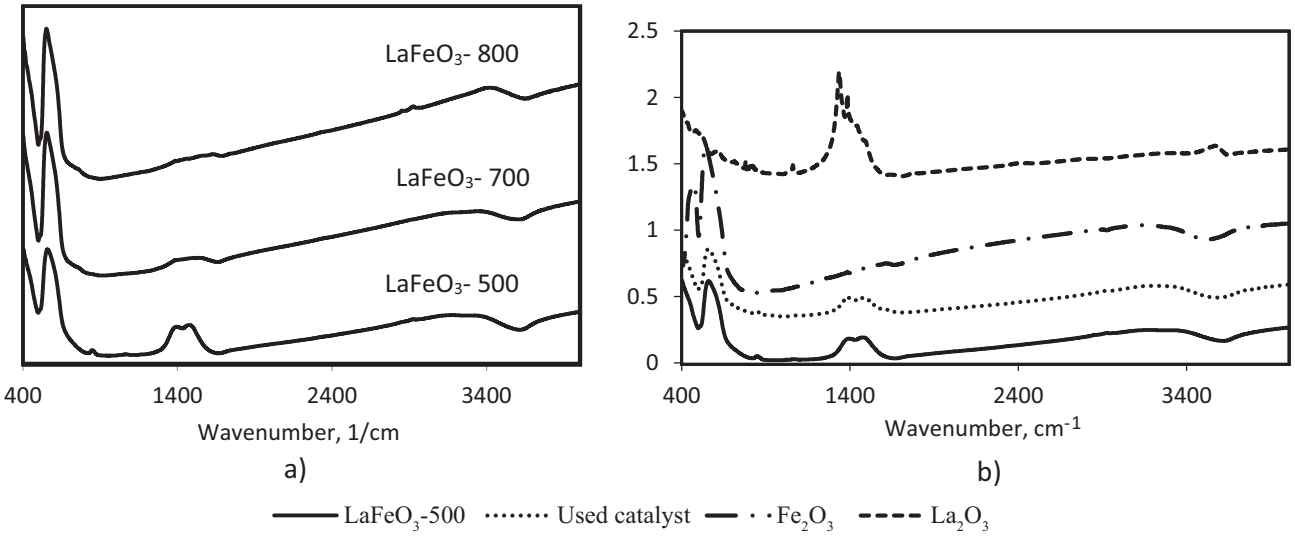

Figure 3. FT-IR spectra of a) perovskite catalysts calcined at 500, 700, and 800 °C, b) used $LaFeO_3$ perovskite, Fe_2O_3, and La_2O_3 samples.

In the spectra, the two strong absorptive bands at about 550 and 400 cm^{-1} were attributed to the Fe–O stretching vibration and O–Fe–O bending vibration mode of the FeO_6 octahedron in the $LaFeO_3$.[14,42,46,48] The broad band at 2900–3400 cm^{-1} corresponds to the surface-adsorbed hydroxyl groups. The two weak bands at 1400 cm^{-1} and 1455 cm^{-1} can be ascribed to the characteristic frequencies of carbonates (Figure 3a). The intensities of these peaks were decreased significantly by increasing calcination temperature. This result indicates that the La-carbonate species ($La_2O_2CO_3$) exist on the $LaFeO_3$ surface at high temperature. The combustion of organic compounds (here citric acid) during the calcination of the catalysts produces CO_2 gas and $LaFeO_3$ is active to chemisorption of CO_2, leading to the formation of carbonates.[46,48] When the FT-IR peaks of La_2O_3 and $LaFeO_3$ are compared, it can be said that lanthanum oxide exists in the $LaFeO_3$ perovskite catalyst. The lanthanum oxide that was not detected by XRD probably exists as nanoparticles or is amorphous

in the perovskite structure.[49] As seen from Figure 3b, the structure of catalyst was preserved when it was used after the sonophoto Fenton-like oxidation of BPA. Although the peak intensities of carbonates groups (at 1400 cm^{-1} and 1455 cm^{-1}) decreased slightly there are no additional peaks in the FT-IR analysis of the catalyst used.

2.1.3. SEM studies

Figure 4 displays the morphology of the $LaFeO_3$ perovskite catalysts, Fe_2O_3, La_2O_3 samples, as well as the SEM images of the $LaFeO_3$-500 catalyst used after sonophoto Fenton-like oxidation of BPA.

The SEM images of the catalyst calcined at 500 °C show that the powders are sponge-like and in the form of porous agglomerates (Figure 4a). At the calcination temperature of 700 °C and 800 °C, it was seen that nanocrystallites were agglomerated, and highly porous layered structures were formed (Figures 4b and 4c). The formation of this porous structure is due to the adding of citric acid during the catalyst preparation step.[43,45,46,48]

When the SEM images of the $LaFeO_3$ perovskite catalyst calcined at 500 °C were compared with the catalyst used after the sonophoto Fenton-like oxidation of BPA (Figures 4a and 4d), it was clear that the pore volume of the catalyst used was increased due to the effect of sonication during the oxidation process of BPA. The SEM images of the Fe_2O_3 catalyst showed a heavily aggregated structure (Figure 4e), whereas the SEM images of the La_2O_3 catalyst presented a layered structure (Figure 4d).

2.1.4. ICP analysis

The content of iron in the samples was determined by ICP-OES analysis (see Table 2).

Table 2. Iron content of the prepared catalysts.

Catalyst	Amount of Fe, ppm
$LaFeO_3$-500	93
$LaFeO_3$-700	94
$LaFeO_3$-800	95

As expected, changing the calcination temperature did not affect the iron content in the catalyst. The calculated theoretical amount of iron was 112 ppm, and the percent error of the iron amount for the catalysts calcined at 500, 700, and 800 °C was 17%, 16%, and 15%, respectively. These small errors may arise from the amount of iron remaining in the laboratory glassware during the catalyst preparation step or from the lack in precision of the ICP-OES analysis device.

2.1.5. Nitrogen adsorption measurements

The BET-surface area (S_{BET}), external surface area (S_{ext}), total pore volume (V_p), mean pore diameter (d_{mean}), and the maximum adsorbed volume obtained from the nitrogen adsorption/desorption measurements are presented in Table 3. Figure 5 displays the nitrogen adsorption studies of the prepared catalysts.

As seen in Table 3, the BET surface area, external surface area, and total pore volume decreased with the increase in the calcination temperature. At the calcination temperature of 800 °C the surface area decreased approximately 5.5-fold. This result may be due to crystal growth and particle agglomeration.[43]

The external surface area of the $LaFeO_3$-500 perovskite used increased from 9.4 m^2/g to 14.2 m^2/g. This result may be due to the reduction of catalyst pore size during the sonication in the oxidation process. This was also confirmed by the SEM images of the samples (Figures 4a and 4d).

The adsorption isotherms, in Figure 5, support these results as well.

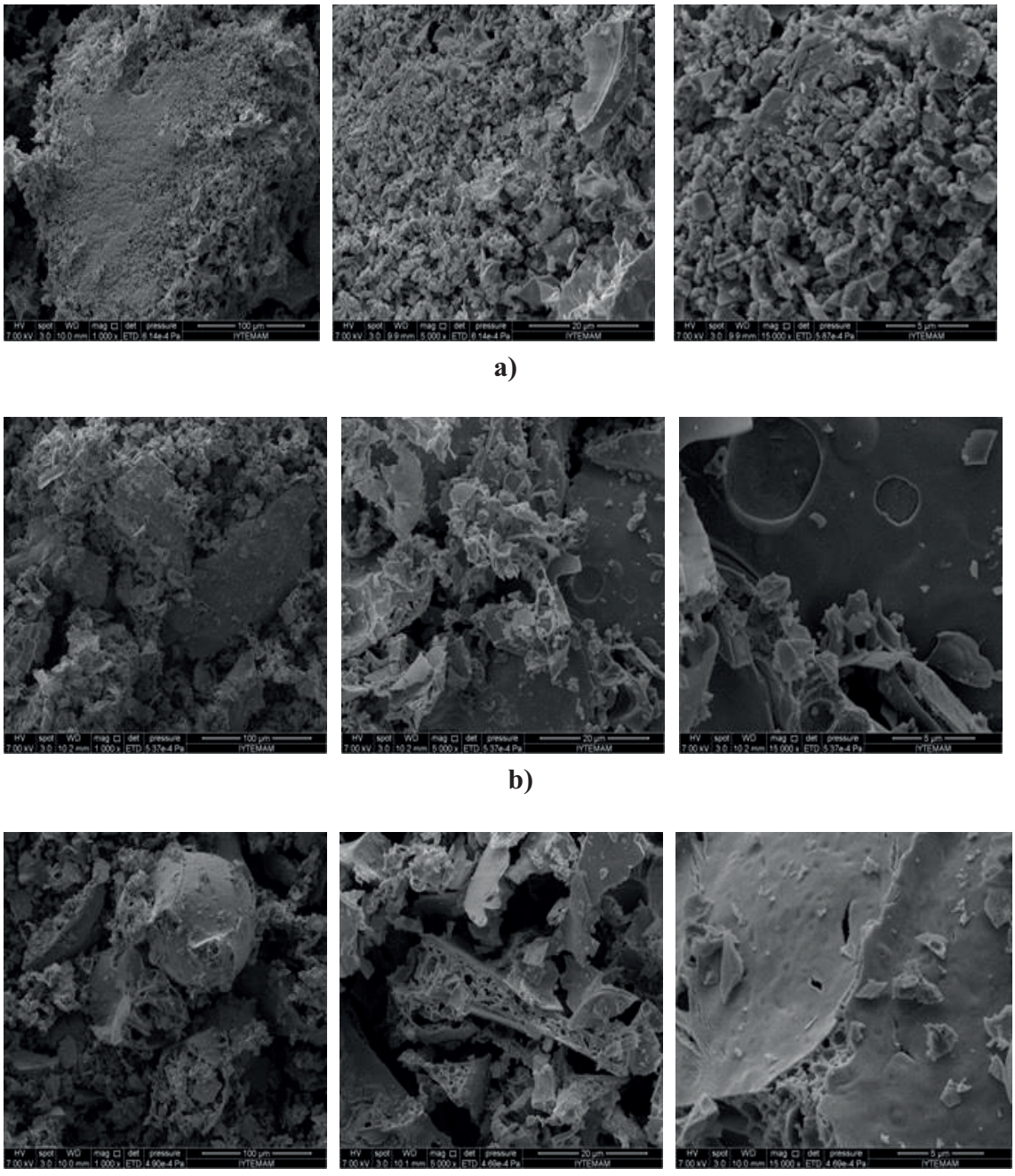

Figure 4. SEM images of the samples: a) $LaFeO_3$-500, b) $LaFeO_3$-700, c) $LaFeO_3$-800.

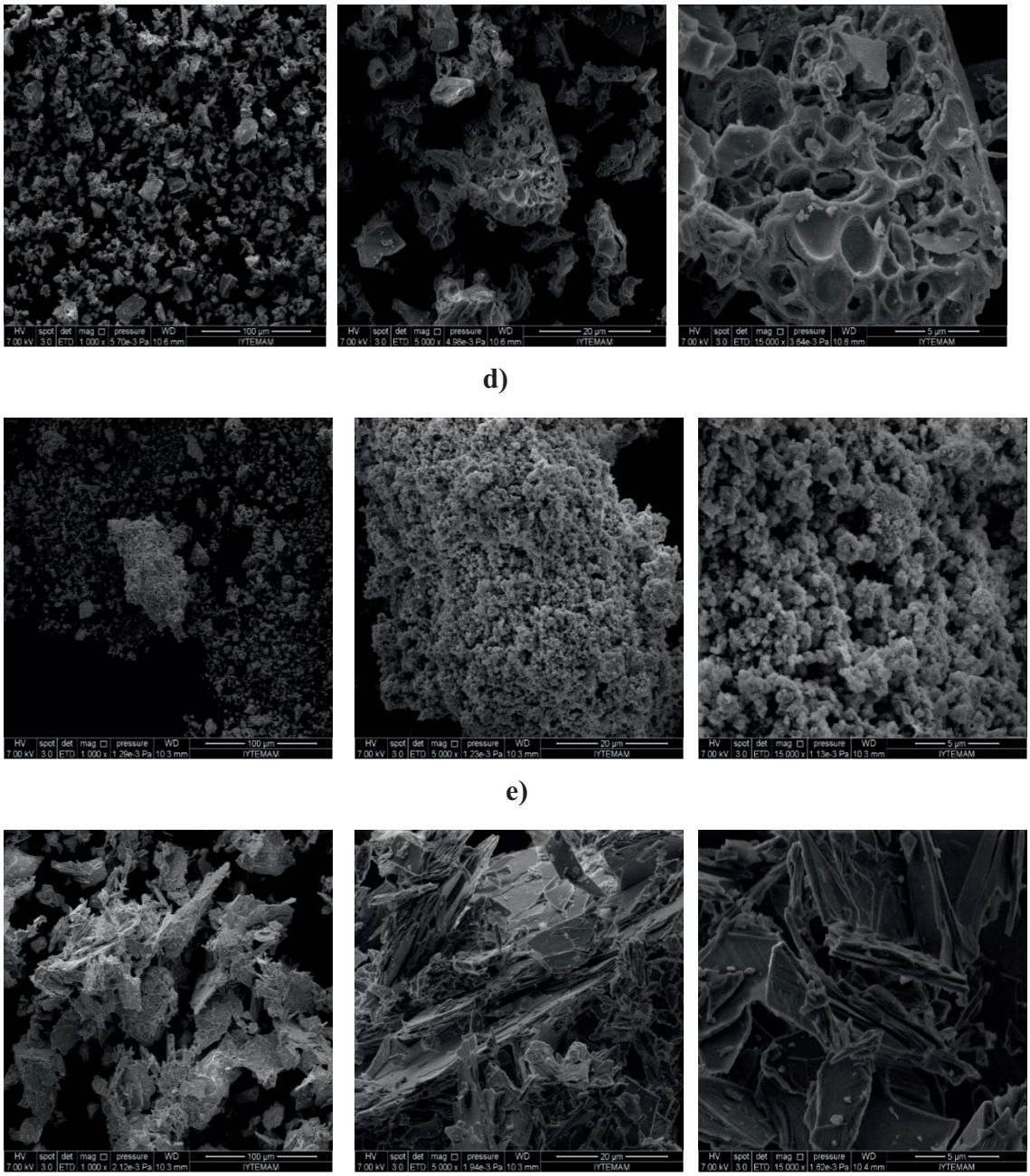

Figure 4. SEM images of the samples: d) $LaFeO_3$-500 (used catalyst), e) Fe_2O_3, f) La_2O_3.

In the literature, Gosavi et al.[45] used three different wet chemistry routes, i.e. co-precipitation, combustion, and sol-gel methods, to prepare $LaFeO_3$ perovskite catalysts. In the mentioned study, the surface areas were 5.4, 9.3, and 16.5 m^2/g and the average pore diameters were 14.0, 20.5, and 11.9 nm, respectively. As seen, the highest BET surface area was achieved with the perovskite catalyst prepared by the sol-gel method. Although the catalyst preparation step was a little different from that in the present study, a similar BET surface area and pore diameter were observed, especially for the catalyst calcined at 500 °C.

Table 3. Surface characteristics of the prepared catalysts.

Catalyst	S_{BET}, m^2/g	S_{ext}, m^2/g	V_p, cm^3/g	$V_{max.}$, cm^3/g	$d^*_{mean.}$, nm
$LaFeO_3$-500	15.4	9.36	0.0052	27.04	11.62
$LaFeO_3$-700	3.61	-	0.0017	2.37	15.59
$LaFeO_3$-800	2.80	-	0.0012	1.04	4.27
$LaFeO_3$-500 (Used catalyst)	15.5	14.2	0.0362	25.14	11.17
La_2O_3	1.4	-	0.0012	0.5614	1.95
Fe_2O_3	13.6	8.6	0.0259	18.17	10.12

*BJH method

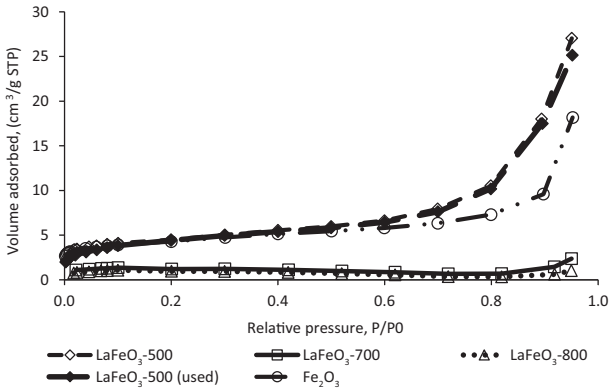

Figure 5. Nitrogen adsorption isotherms of the prepared catalysts.

According to IUPAC classification, the N_2 adsorption isotherm of the catalyst calcined at 500 °C is of type V isotherms with type H3 hysteresis loops in the relative pressure (P/P_0) range of 0.6–1.0. This shows that the prepared catalyst contains mesopores. On the other hand, there was a certain amount of gas adsorbed at the initial point of the relative pressure for the catalyst calcined at 500 °C, revealing the existence of micropores in that catalyst.[50] Similarly, the catalysts calcined at 700 and 800 °C show type V isotherms with type H3 hysteresis loops in the relative pressure (P/P_0) range of 0.6–1.0. The Fe_2O_3 sample shows type V isotherms with type H3 hysteresis loops in the relative pressure (P/P_0) range of 0.8–1.0. The nitrogen adsorption isotherm of the La_2O_3 sample could not be given because of the low surface area of the La_2O_3 sample (1.4 m^2/g).

In the literature, the $EuFeO_3$ perovskite catalyst prepared by a sol-gel method shows type V isotherms with type H3 hysteresis loops.[14] Similarly, the nitrogen adsorption isotherms of the $LaMnO_3$ perovskite catalysts synthesized with citrate sol-gel, glycine combustion, or the co-precipitation methods were characterized by the combination of microporous and mesoporous structures with type H3 hysteresis loops in the relative pressure range of 0.6–1.0.[50]

2.1.6. Diffuse reflectance spectra of the prepared catalysts

The UV-Vis diffuse reflectance spectra of the perovskite catalysts calcined at three different temperatures, and the Fe_2O_3, and La_2O_3 samples are presented in Figures 6 and 7, respectively. A modified Kubelka–Munk function (Eq. (12)) was used for determining the band gap energy (E_g) of the prepared samples:

$$(F(R) \times hv)^{1/n} = B(hv - E_g), \tag{12}$$

where h is Planck's constant, v is the light frequency, B is a constant, $F(R) = (1 - R)^2/2R$, R is reflectance, and $hv = (1240/\lambda)$ eV. Values of n can be different depending on the type of electronic transition, where n = 2 for an indirect allowed transition and n = 1/2 for a direct allowed transition.[51] In this study, indirect transition, n = 2, is used. Figures 6 and 7 plot the $(F(R) \times hv)^{1/n}$ versus the hv curve. The value of the band gap energy (E_g) can be obtained by extrapolating the linear part of the curve to the horizontal axis (hv axis). The indirect type transition showed band gap values of 1.3, 1.5, and 1.7 eV for the catalysts $LaFeO_3$-500, $LaFeO_3$-700, and $LaFeO_3$-800, respectively.

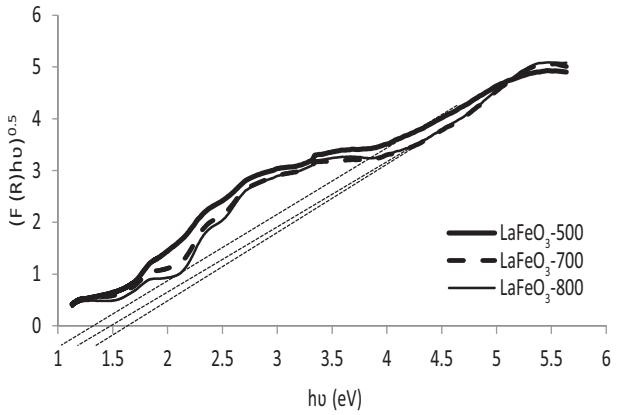

Figure 6. UV-Vis diffuse reflectance spectra of the $LaFeO_3$-500, $LaFeO_3$-700, and $LaFeO_3$-800 perovskite catalysts.

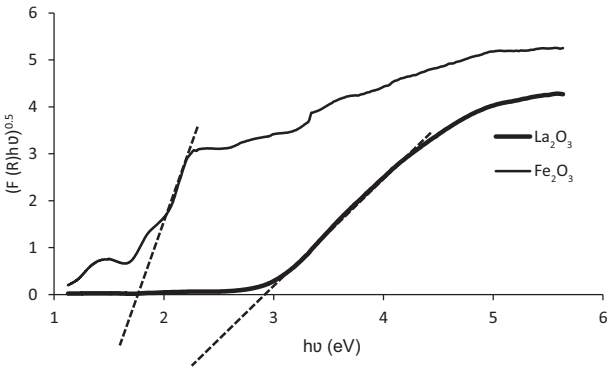

Figure 7. UV-Vis diffuse reflectance spectra of the Fe_2O_3 and La_2O_3 catalysts.

The perovskite catalysts have low band gap energy, which increases the photocatalytic activity in visible light. In the literature, band gap energies for $LaFeO_3$ perovskite catalysts were reported to be 2.0 and 2.1 eV.[52,53]

As seen from Figure 6, the band gap energies increased with an increasing calcination temperature. Similar results were obtained in the study done by Ju et al.[14] In that study, the band gap energies of the $EuFeO_3$ perovskite catalyst calcined at 700, 750, and 800 °C were 2.15, 2.22, and 2.25 eV, respectively.

The band gap energies of the La_2O_3 and Fe_2O_3 catalyst were 2.95 and 1.8, respectively (Figure 7). In a study done by Souza et al.,[54] the calculated band gap energy for Fe_2O_3 was in the range of 1.73–1.80 eV. The high band gap energy for La_2O_3 shows that La_2O_3 can be more active under UV light rather than under visible light.

2.2. Sonophoto Fenton-like oxidation of BPA over $LaFeO_3$ perovskite catalysts

Catalytic activity studies (for determining the best active catalyst in sonophoto Fenton-like oxidation of BPA) were carried out under the following conditions: 15 ppm BPA aqueous solution (66 μM), initial BPA pH around 6.7, solution volume of 0.5 dm^3, catalyst amount of 0.5 g/dm^3, H_2O_2 amount of 2.38 mM, stirring speed of 500 rpm, temperature of 298 K, reaction duration of 180 min in the presence of sonication, and visible light lamps. The selected concentration of H_2O_2 is the stoichiometric amount to achieve complete mineralization of BPA according to the equation below:

$$C_{15}H_{16}O_2 + 36H_2O_2 \rightarrow 15CO_2 + 44H_2O \quad (13)$$

At the beginning of each run to establish the adsorption/desorption equilibrium of BPA over the catalyst, a known concentration of BPA was stirred in the dark (in the absence of light, sonication, and H_2O_2) at 298 K. The reaction vessel was kept in a box to avoid photochemical reactions induced by natural light. At the end of 30 min, a sample was taken from the solution and analyzed by HPLC. Then the experiment was initiated with the switching on of the light and sonication and with addition of H_2O_2. Samples were periodically drawn from the vessel, and the reaction was stopped by putting the samples in iced-water. After centrifugation and filtration with PTFE syringe filters (0.45 μm), the samples were subjected to analysis.

Each run was repeated at least 3 times and the standard deviation of the average of independent runs varied in the range of ± 0.01 and ± 2.1.

Figure 8 represents the activities of the $LaFeO_3$ perovskite catalysts calcined at three different temperatures in the sonophoto Fenton-like oxidation of BPA.

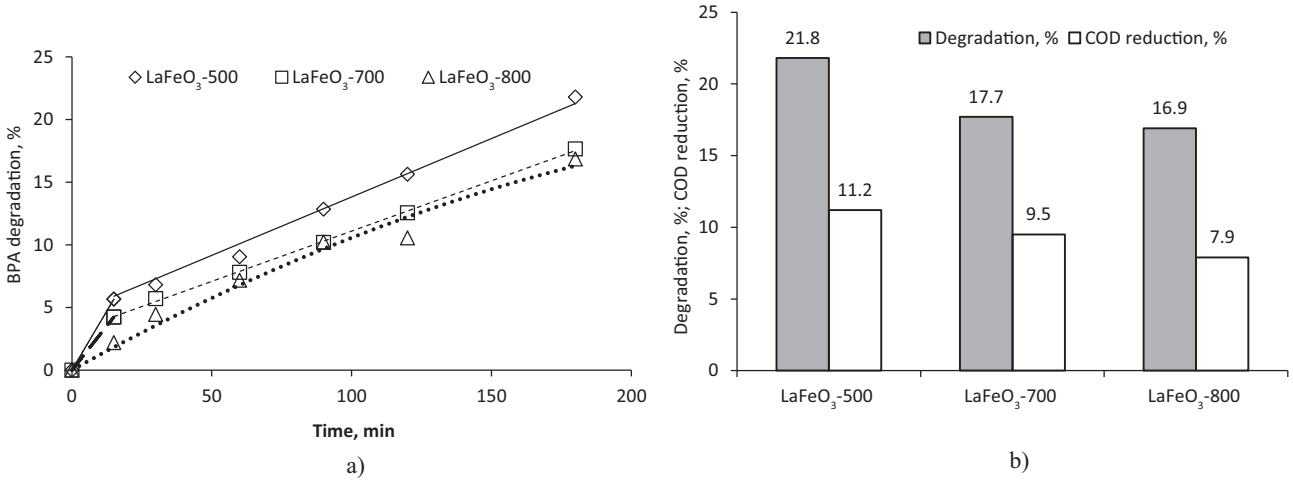

Figure 8. Sonophoto Fenton-like oxidation of BPA over the prepared catalysts: a) Degradation, % vs. time and b) Degradation, % and COD reduction % at the end of 3 h.

The adsorption of BPA at the end of 30 min was small enough to be ignored, 2.2%. The initial concentration shown in Figure 8a is the concentration at the end of 30 min of adsorption just after the addition of H_2O_2.

As seen from Figures 8a and 8b, the most active catalyst in terms of degradation and COD reduction was the one calcined at 500 °C. The degradation of BPA and COD reduction decreased with the increasing calcination temperature. As mentioned in the catalyst characterization studies, crystal size increased and surface area decreased with an increase in the calcination temperature, which decreases the BPA degradation due to the reduction in the adsorption of BPA over the catalyst surface. It is well known that smaller particle size with higher surface area provides more active sites and is favorable for photocatalytic reactions.[42,55] The smaller the crystal size, the higher the photocatalytic activity, which can be explained as follows: a) the smaller the crystal size, the stronger the oxidizing capability of the photoinduced holes and the reducing capability of photoinduced electrons (Eqs. (3) and (4)), which provides more hydroxyl radicals, and b) the migrating time of photoinduced charge carriers from the inner areas to the surfaces is short if the crystal size is small. Thus, photoinduced charge carriers have the chance to reach the surfaces in advance of recombination, to be further captured and then these carriers can initiate the photochemical reactions.[11] In the present study, the crystal sizes of the

catalysts calcined at 500, 700, and 800 °C were 19.69, 28.51, and 41.35 nm, respectively (Table 1). In addition, the BET surface areas of the mentioned catalysts were 15.4, 3.61, and 2.80 m^2/g, respectively. The values of the band gap energies of the samples calcined at 500, 700, and 800 °C were 1.3, 1.5, and 1.7 eV, respectively. The sample exhibits lower optical absorption ability in the visible light range with the increase in the band gap energy.[14,56] As a consequence, it can be said that the catalyst characterization results are in good agreement with the catalytic activity results.

The TOC reduction was measured at the end of 3 h of oxidation as well, but no TOC reduction was observed, which showed that 3 h of oxidation was not enough to degrade BPA into CO_2 (Eq. (5)).

The activity and stability of the catalyst are critical parameters and have major importance, particularly for industrial processes. In the present study, the stability of the catalysts was tested by measuring the amount of iron dissolved in the solution (the iron leaching) after the oxidation using an atomic absorption spectrometer (Varian 10 plus). The amount dissolved in the solution after oxidation was 0.17 (0.18%), 0.15 (0.16%), and 0.15 (0.16%) ppm for the catalysts calcined at 500, 700, and 800 °C, respectively. As can be seen, the amount is below that given in E.U. directives (<2 mg/dm^3). In addition to this measurement, the reusability of the most active catalyst ($LaFeO_3$ perovskite catalyst calcined at 500 °C) was tested. For this purpose, to recover the catalyst, after 180 min of sonophoto Fenton-like oxidation, the final effluent was filtrated. The used catalyst was washed with water and then ethanol, then dried at 120 °C for 3 h, and calcined at 500 °C for 6 h. The calcined catalyst was tested in the sonophoto Fenton-like degradation of BPA under the same conditions described above. Degradation of 20.5% was obtained with used catalyst after 3 h of oxidation. As seen, similar degradation was obtained for fresh (21.8%) and used catalyst (20.5%) after 3 h of oxidation. These results show that the catalyst has good stability and the process is mainly the heterogeneous sonophoto Fenton-like process, instead of the homogeneous sonophoto Fenton-like process.

2.3. Activity of the Fe/TiO_2 catalyst in the sonophoto Fenton-like oxidation of BPA under visible light

The heterogeneous sonophoto Fenton-like oxidation of BPA was also investigated over Fe containing a TiO_2 catalyst (1 wt% Fe/TiO_2) and the obtained result was compared with the catalytic activity of the $LaFeO_3$ perovskite catalyst.

The experimental conditions were the same as those mentioned in Part 3.2, but the reaction duration was 6 h (instead of 3 h), which enabled a measurable TOC reduction to be obtained.

It is well known that TiO_2 is the most commonly used semiconductor photocatalyst because of its relatively high photocatalytic activity, chemical stability, low cost, and environmental friendliness. In the present study, the Fe-containing TiO_2 catalyst prepared with the sol-gel method was used. However, TiO_2 is active only under UV light irradiation due to its large band gap energy (3.2 eV), which results in low efficiency in terms of use of solar light.[8,9] In order to enhance the photocatalytic activity of TiO_2 under visible light, significant efforts have been made in the past decades, such as iron doping.[57] The presence of Fe^{3+} in the catalyst also acts as a Fenton-like catalyst and helps the production of more hydroxyl radicals.[58] Iron doping decreased the bang gap of the bare TiO_2, as well. In the present study, the bang gap energies of the bare TiO_2 and Fe/TiO_2 were 3.0 eV and 2.3 eV, respectively, which are larger than that of the $LaFeO_3$ perovskite catalyst calcined at 500 °C (1.3 eV). Although the Fe/TiO_2 catalyst has a larger surface area (58.9 m^2/g) than that of the $LaFeO_3$-perovskite catalyst calcined at 500 °C (15.4 m^2/g), higher photocatalytic activity of

the $LaFeO_3$-500 catalyst in the oxidation of BPA under visible light was observed. As seen from Figure 9, the degradation of BPA, COD, and TOC reductions after 6 h of oxidation were 34.8%, 26.9%, and 8.8% for the $LaFeO_3$ perovskite catalyst and were 33.1%, 19.7%, and 4.9% for the Fe/TiO_2 catalyst, respectively. According to this result, it may be said that band gap energy plays a more important role than surface area does under the experimental conditions used in this study.

Figure 9 shows a comparison of the activity of the $LaFeO_3$ perovskite catalyst with the Fe/TiO_2 catalyst in the sonophoto Fenton-like oxidation of BPA.

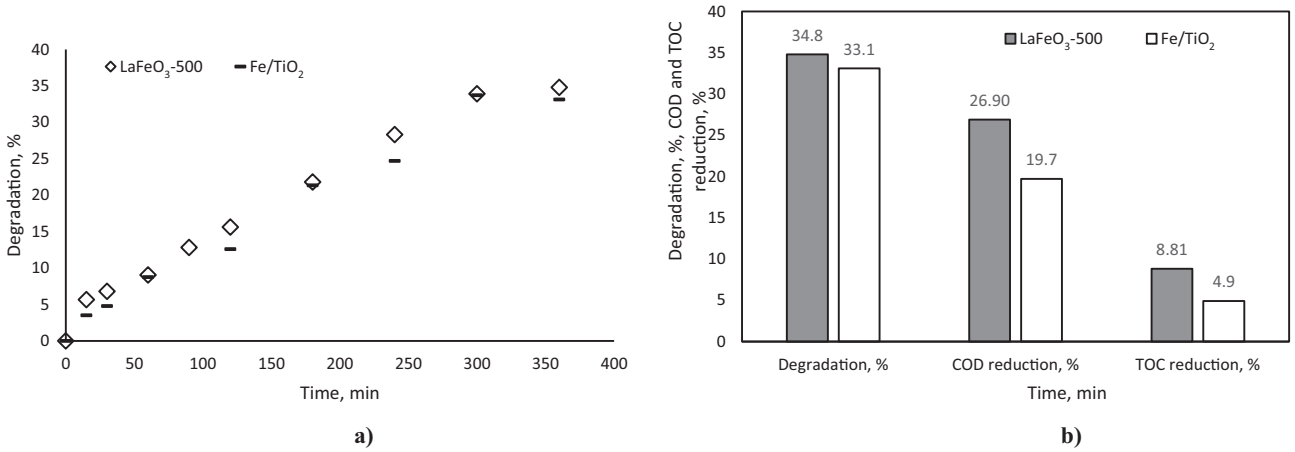

Figure 9. Comparison of the activity of the $LaFeO_3$ perovskite catalyst with the Fe/TiO_2 catalyst in the sonophoto Fenton-like oxidation of BPA: a) Degradation, % vs. time and b) Degradation, %, COD and TOC reductions % at the end of 6 h.

3. Experimental

3.1. Catalyst preparation

3.1.1. Preparation of $LaFeO_3$ perovskite catalyst

The $LaFeO_3$ perovskite catalysts were prepared with the sol-gel preparation method.[59] $Fe(NO_3)_3.9H_2O$ (Aldrich), $La(NO_3)_3.6\ H_2O$ (Fluka), and citric acid ($C_6H_8O_7.H_2O$, Merck) were used as raw materials. The gel precursor was prepared as follows: 0.015 mol $Fe(NO_3)_3.9H_2O$, 0.015 mol $La(NO_3)_3.6\ H_2O$, and 0.05 mol citric acid were dissolved in 100 mL of ultrapure water. The solution was stirred at 80 °C for 3 h, and then heated at the same temperature to evaporate the water. The gel precursor was dried in air for 3 h at 120 °C, and then the resulting material was calcined at 500 °C, 700 °C, and 800 °C for 6h. The prepared samples were denoted as $LaFeO_3$-500, $LaFeO_3$-700, and $LaFeO_3$-800, respectively.

For the comparison of the structure of $LaFeO_3$-500 perovskite catalyst with Fe_2O_3 and La_2O_3 samples, the Fe_2O_3 and La_2O_3 samples were prepared as follows: $Fe(NO_3)_3.9H_2O$ or $La(NO_3)_3.6\ H_2O$ was dried in air for 3 h at 120 °C, and then the resulting material was calcined at 500 °C for 6 h.[59]

3.1.2. Preparation of 1 wt% Fe/TiO_2 catalyst

First 20 mL of $Ti(OC_4H_9)_4$ was added dropwise to 80 mL of absolute ethanol under vigorous stirring (350 rpm). Then an appropriate amount of $Fe(NO_3)_3.9H_2O$ was dissolved in ultrapure water and this solution

was slowly added to the titanium mixture. Afterward, the obtained solution was added dropwise to a mixture containing 80 mL of ethanol, 3 mL of distilled water, and 8 mL of acetic acid under vigorous stirring. The resulting transparent colloidal suspension was stirred for 2 h and aged for 11 days until the formation of a gel. The gel was dried at 80 °C for 48 h, followed by calcination at 500 °C for 3 h.[9]

3.2. Experimental procedure for the heterogeneous sonophoto Fenton-like oxidation of BPA

The experiments were carried out in the experimental set-up shown in Figure 10. In a typical experiment, 0.5 dm^3 of 15 ppm (66 μM) of BPA aqueous solution was poured into the cylindrical reactor and 0.5 g/dm^3 of catalyst was added to the solution and the suspension was left for 30 min in the dark to establish the adsorption–desorption equilibrium of the BPA on the catalyst surface. The amount of BPA adsorbed by the catalyst was determined by measuring the BPA concentration after 30 min in the absence of visible light illumination, sonication, and H_2O_2. Then H_2O_2 was added and the visible light lamps and ultrasound (US, frequency of 20 kHz and at an input power of 40 W, Bandelin HD3200) were turned on. The solution was irradiated with two visible lamps (high pressure Na lamps, each 150 W, Philips). The heterogeneous sonophoto Fenton-like process for the degradation of BPA took 3 h or 6 h. The reaction temperature was kept constant at 298 ± 2 K by circulating cooling water (PolyScience, MX07R-20-A12E) around the reactor to avoid significant overheating of the reaction media. The reaction vessel was kept in a box to avoid photochemical reactions induced by natural light. The experiments were performed at a BPA ambient pH, which was about 6.7 and left uncontrolled during the experiments. Samples were periodically drawn from the vessel and centrifuged for 15 min and were filtrated with 0.45 μm PTFE (Agilent) syringe filters and then analyzed by HPLC (Agilent 1200) with a ZORBAX Eclipse Plus C18 (4.6 × 150 mm, 5 μm) column. Detection was achieved with an UV detector at 278 nm, with a 20 μL sampling loop. The mobile phase, ultrapure water/acetonitrile (50/50, v/v), was run in isocratic mode with a flow rate of 0.5 mL/min. The column oven was maintained at 25 °C.

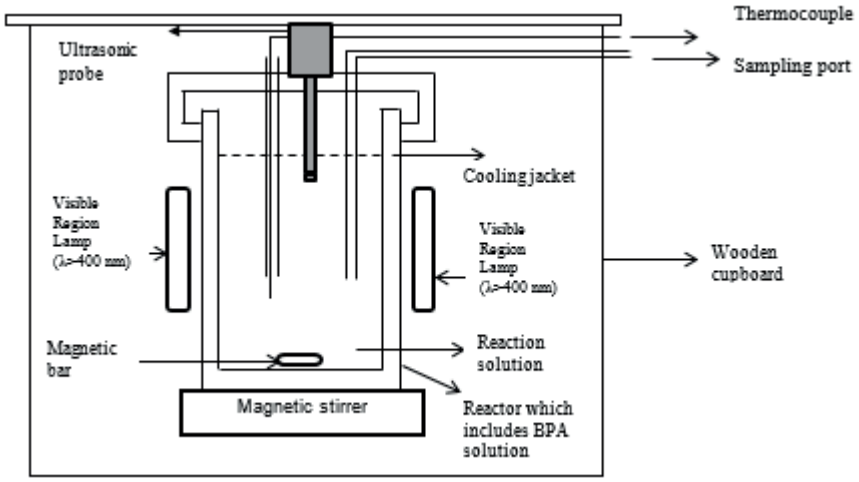

Figure 10. Experimental set-up used for the heterogeneous sonophoto Fenton-like oxidation process.

In addition to these measurements, the chemical oxygen demand (COD) removal of the BPA solution was determined by measuring initial COD and final COD (at the end of the run) of the BPA solution with a COD device (Lovibond Checkit Direct COD Vario). The total organic carbon (TOC) reduction was measured with a Teledyne Tekmar Lotix analyzer at the end of each experiment.

4. Conclusions

This study shows that the combination of ultrasound and visible light illumination with the heterogeneous Fenton-like process was efficient for the degradation of bisphenol-A (BPA) in the presence of an iron-containing $LaFeO_3$ perovskite catalyst. Increasing the catalyst calcination temperature caused a decrease in activity. The photocatalytic activity of the $LaFeO_3$-500 catalyst was higher than that of the iron-containing TiO_2 catalyst in the oxidation of BPA under visible light. According to the results obtained from this study, it may be said that the band gap energy of the catalysts plays a more important role than did the surface area of the catalysts under visible light at the experimental conditions used.

After 6 h of reaction, the sonophoto Fenton-like oxidation system appears to be a promising process for BPA-containing synthetic wastewater treatment with BPA degradation of 34.8%, COD removal of 26.9%, and TOC removal of 8.8% in the presence of a $LaFeO_3$ perovskite catalyst. These removal degrees may be increased by changing the studied experimental conditions.

Acknowledgments

The author acknowledges the financial support from the Scientific and Technological Research Council of Turkey (TÜBİTAK) under project number 213M648 and Ege University Scientific Research Fund under projects no. 14MÜH034 and 15BİL009. The author also acknowledges the assistance and guidance of Professor Gönül Gündüz during this study.

References

1. Kuo, C. Y.; Hsiao, H. M. *Process. Saf. Environ.* **2015**, *95*, 265-270.
2. Sharma, J.; Mishra, I. M.; Kumar, V. *J. Environ. Manage.* **2015**, *156*, 266-275.
3. Crain, D. A.; Eriksen, M.; Iguchi, T.; Jobling, S.; Laufer, H.; Leblanc, G. A.; Guillette, L. J. *Reprod. Toxicol.* **2007**, *24*, 225-239.
4. Er, B.; Sarımehmetoğlu, B. *Vet. Hekim Derg.* **2011**, *82*, 69-74.
5. Luoa, L.; Yang, Y.; Zhang, A.; Wang, M.; Liu, Y.; Bian, L.; Jiang, F.; Pan, X. *Appl. Surf. Sci.* **2015**, *353*, 469-479.
6. Zhang, K.; Gao, N.; Deng, Y.; Lin, T. F.; Ma, Y.; Li, L.; Sui, M. *J. Environ. Sci.* **2011**, *23*, 31-36.
7. Dükkancı, M.; Gündüz, G.; Yılmaz, S.; Yaman, Y. C.; Prihod'ko, R. V.; Stolyarova, I. V. *Appl. Catal. B-Environ.* **2010**, *95*, 270-278.
8. Bolova, E.; Gündüz, G.; Dükkancı, M.; Yılmaz, S.; Yaman, Y. C. *Int. J. Chem. React Eng.* **2011**, *9*, 1-20.
9. Sun, S.; Ding, J.; Bao, J.; Gao, C.; Zeming, Q.; Yang, X.; He, B.; Li, C. *Appl. Surf. Sci.* **2012**, *258*, 5031-5037.
10. Pelaez, M.; Nolan, N. T.; Pillai, S. C.; Seery, M. K; Falaras, P.; Kontos, A. G.; Dunlop, P. S. M.; Hamilton, J. W. J.; Byrne, J. A.; O'Shea, K.; et al. *Appl. Catal. B-Environ.* **2012**, *125*, 331-349.
11. Li, S.; Jing, L.; Fu, W.; Yang, L.; Xin, B.; Fu, H. *Mater. Res. Bull.* **2007**, *42*, 203-212.
12. Chen, L.; Huang, R.; Yin, S.; Luo, S.; Au, C. *Chem. Eng. J.* **2012**, *193-194*, 123-130.
13. Dong, B.; Li, Z.; Li, Z.; Xu, X.; Song, M.; Zheng, W.; Wang, C.; Al-Deyab, S. S.; El-Newehy, M. *J. Am. Ceram. Soc.* **2010**, *93*, 3587-3590.
14. Ju, L.; Chen, Z.; Fang, L.; Dong, W.; Zheng, F.; Shen, M. *J. Am. Ceram. Soc.* **2011**, *94*, 3418-3424.
15. Dükkancı, M. PhD, Chemical Engineering Department, Ege University, Turkey, 2015.
16. Petrier, C.; Torres-Palma, R.; Combet, E.; Sarantakos, G.; Baup, S.; Pulgarin, C. *Ultrason. Sonochem.* **2010**, *17*, 111-115.

17. Son, Y.; Lim, M.; Khim, J.; Kim, L. H.; Ashokkumar, M. *Chem. Eng. J.* **2012**, *183*, 39-45.
18. Torres, R. A.; Abdelmalek, F.; Combet, E.; Petrier, C.; Pulgarin, C. *J. Hazard. Mater.* **2007**, *146*, 546-551.
19. Mohapatra, D. P.; Brar, S. K.; Tyagi, R. D.; Surampalli, R. Y. *Ultrason. Sonochem.* **2011**, *18*, 1018-1027.
20. Huang, R.; Fang, Z.; Yan, X.; Cheng, W. *Chem. Eng. J.* **2012**, *197*, 242-249.
21. Katsumata, H.; Kawabe, S.; Kaneco, S.; Suzuki, T.; Ohta, K. *J. Photoch. Photobio. A.* **2004**, *162*, 297-305.
22. Lin, K.; Ding, J.; Wang, H.; Huang, X.; Gan, J. *Chemosphere* **2012**, *89*, 789-795.
23. Zhou, D.; Wu, F.; Deng, N.; Xiang, W. *Water. Res.* **2004**, *38*, 4107-4116.
24. Neamtu, M.; Frimmel, F. H. *Water Res.* **2006**, *40*, 3745-3750.
25. Kuo, C.; Wu, C.; Lin, H. *Desalination.* **2010**, *256*, 37-42.
26. Wang, X.; Lim, T. *Appl. Catal. B-Environ.* **2010**, *100*, 355-364.
27. Qing, Z.; Jinhua, L.; Hongchong, C.; Quanpeng, C.; Baoxue, Z.; Shuchuan, S.; Weimin, C. *Chinese J. Catal.* **2011**, *32*, 1357-1363.
28. Yang, J.; Dai, J.; Li, J. *Appl. Surf. Sci*, **2011**, *257*, 8965-8973.
29. Irmak, S.; Erbatur, O.; Akgerman, A. *J. Hazard. Mater.* **2005**, *B126*, 54-62.
30. Deborde, M.; Rabouan, S.; Mazellier, P.; Duguet, J. P.; Legube, B. *Water Res.* **2008**, *42*, 4299-4308.
31. Garoma, T.; Matsumoto, S. *J. Hazard. Mater.* **2009**, *167*, 1185-1191.
32. Torres-Palma, R. A.; Nieto, J. I.; Combet, E.; Petrier, C.; Pulgarin, C. *Water Res.* **2010**, *44*, 2245-2252.
33. Lim, M.; Son, Y.; Na, S.; Khim, J. Effect of TiO_2 Concentration for Sonophotocatalytic Degradation of Bisphenol A. *Proceedings of Symposium on Ultrasonic Electronics*, **2010**, *31*, 103-104.
34. Poerschmann, J.; Trommler, U.; Gorecki, T. *Chemosphere* **2010**, *79*, 975-986.
35. Leiw, M. Y.; Guai, G. H.; Wang, X.; Tse, M. S.; Mang, N. C.; Tan, O. K. *J. Hazard. Mater.* **2013**, *260*, 1-8.
36. Xie, Y. B.; Li, X. Z. *J. Hazard. Mater.* **2006**, *B38*, 526-533.
37. Wang, C.; Zhu, L.; Song, C.; Shan, G.; Chen, P. *Appl. Catal. B - Environ.* **2011**, *105*, 229-236.
38. Wang, C.; Zhu, L.; Wei, M.; Chen, P.; Shan, G. *Water Res.* **2012**, *46*, 845-853.
39. Xing, R.; Wu, L.; Fei, Z.; Wu, P. *J. Environ. Sci.* **2013**, *25*, 1687-1695.
40. Zhang, L.; Wang, W.; Sun, S.; Sun, Y.; Gao, E.; Zhang, Z. *Appl. Catal. B-Environ.* **2014**, *148-149*, 164-169.
41. Wang, C.; Zhu, J.; Wu, X.; Xu, H.; Song, Y.; Yan, J.; Song, Y.; Ji, H.; Wang, K.; Li, H. *Ceram. Int.* **2014**, *40*, 8061-8070.
42. Hu, R.; Li, C.; Wang, X.; Sun, Y.; Jia, H.; Su, H.; Zhang, Y. *Catal. Commun.* **2012**, *29*, 35-39.
43. Sun, M.; Jiang, Y.; Li, F.; Xia, M.; Xue, B.; Liu, D. *Mater. Trans.* **2010**, *51*, 2208-2214.
44. Faye, J.; Guelou, E.; Barrault, J.; Tatibouet, J. M.; Valange, S. *Top. Catal.* **2009**, *52*, 1211-1219.
45. Gosavi, P. V.; Biniwale, R. B. *Mat. Chem. Phys.* **2010**, *119*, 324-329.
46. Wei, Z. X.; Xu, Y. Q.; Liu, H. Y.; Hu, C. W. *J Hazard. Mater.* **2009**, *165*, 1056-1061.
47. Tayade, R. J.; Surolia, P. K.; Kulkarni, R. G.; Jasra, R. V. *Sci. Technol. Adv. Mat.* **2007**, *8*, 455-462.
48. Ding, J.; Lü, X.; Shu, H.; Xie, J.; Zhang, H. *Mater. Sci. Eng. B-Adv.* **2010**, *171*, 31-34.
49. Cho, Y. G.; Choi, K. H.; Kim, Y. R.; Jung, J. S.; Lee, S. H. *Bull. Korean Chem. Soc.* **2009**, *30*, 1368-1372.
50. Zhang, C.; Guo, Y.; Guo, Y.; Lu, G.; Boreave, A.; Retailleau, L.; Baylet, A.; Giroir-Fendler, A. *Appl. Catal. B-Environ.* **2014**, *148*, 490-498.
51. Mi, J. L.; Johnsen, S.; Clausen, C.; Hald, P.; Lock, N.; So, L.; Iversen, B. B. *J. Mater. Res.* **2012**, *28*, 333-338.
52. Scafetta, M. D.; Xie, Y. J.; Torres, M.; Spaner, J. E.; May, S. *J. Appl. Phys. Lett.* **2013**, *102*, 081904-1-5.
53. Erat, S.; Wadati, H.; Aksoy, F.; Liu, Z.; Graule, T.; Gauckler, L. J.; Braun, A. *Appl. Phys. Lett.* **2010**, *97*, 124101.

54. Souza, F. L.; Lopes, K. P.; Longo, E.; Leite, E. R. *Phys. Chem. Chem. Phys.* **2009**, *11*, 1215-1221.

55. Li, Y.; Yao, S.; Wen, W.; Xue, L.; Yan, Y. *J. Alloy. Compd.* **2010**, *491*, 560-564.

56. Ganesh, I.; Kumar, P. P.; Gupta, A. K.; Sekhar, P. S. C.; Radha, K.; Padmanabham, G.; Sundararajan, G. *Process. Appl. Ceram.* **2012**, *6*, 21-36.

57. Lezner, M.; Grabowska, E.; Zaleska, A. *Physicochem. Probl. Mi.* **2012**, *48*, 193-200.

58. Ünnü, B. A.; Gündüz, G.; Dükkancı, M. *Desalin. Water Treat.* **2016**, *57*, 11835-11849.

59. Yang, M.; Xu, A.; Du, H.; Sun, C.; Li, C. *J. Hazard. Mater.* **2007**, *B139*, 86-92.